

equivalent to all of the binding energy released from fusing He converted into kinetic energy (because the star is assumed to be left bound). We infer for SN 2002bj photospheric velocities that drop rapidly from about 8400 km s^{-1} at detection to 2000 km s^{-1} 3 weeks later. Extrapolating to an explosion date 7 days before detection, the initial velocity could have been between $14,000 \text{ km s}^{-1}$ (linear extrapolation) and $\sim 25,000 \text{ km s}^{-1}$ [exponential extrapolation as often seen in SNe (17, 18)]. A rise time that is faster by a factor of 2 would imply velocities twice as high. The only direct measurement we have is from the spectrum 7 days after detection: about 4000 km s^{-1} . This is consistent with the derived photospheric velocity at that time if the rise time was about 7 days.

Out to a distance of 60 Mpc, the LOSS survey is complete (99%) for SNe Ia, and 31 have been found. Because SN 2002bj is quite luminous, the incompleteness correction for it is almost as small (94%), resulting in a relative rate of 3.4% of the SN Ia rate for SN 2002bj-like SNe (19). This is in good agreement with the predictions for SNe Ia.

The SN Ia model, still in its infancy, lacks more stringent predictions such as detailed light curves and spectral composition and evolution. Nevertheless, all the diagnostics we could apply seem consistent with this interpretation. The evidence here is tentative, but the existence of V, if seen in future discoveries of objects of this class, points to a different nucleosynthetic chain and

therefore may serve as a smoking gun for a truly different SN explosion channel. Regardless of the interpretation, current and future surveys should focus on short cadences—repeat visits on daily rather than weekly time scales—in order to find many more SNe resembling SN 2002bj.

References and Notes

1. A. V. Filippenko, *Annu. Rev. Astron. Astrophys.* **35**, 309 (1997).
2. T. Puckett, J. Newton, M. Papenkova, W. D. Li, *IAU Circ.* **7839**, 1 (2002).
3. The blue continuum, in combination with residual host galaxy lines, explains the original erroneous classification of this object as a SN II on the basis of a noisier spectrum (20).
4. D. A. Howell *et al.*, *Nature* **443**, 308 (2006).
5. M. Hicken *et al.*, *Astrophys. J. Lett.* **669**, L17 (2007).
6. M. Yamanaka *et al.*, <http://arxiv.org/abs/0908.2059> (2009).
7. A. Fisher, D. Branch, P. Nugent, E. Baron, *Astrophys. J. Lett.* **481**, L89 (1997).
8. W. D. Arnett, *Astrophys. J.* **253**, 785 (1982).
9. P. G. Sutherland, J. C. Wheeler, *Astrophys. J.* **280**, 282 (1984).
10. L. Bildsten, K. J. Shen, N. N. Weinberg, G. Nelemans, *Astrophys. J. Lett.* **662**, L95 (2007).
11. K. J. Shen, L. Bildsten, *Astrophys. J.* **699**, 1365 (2009).
12. H. B. Perets *et al.*, <http://arxiv.org/abs/0906.2003> (2009).
13. S. Valenti *et al.*, *Nature* **459**, 674 (2009).
14. R. J. Foley, *et al.*, *Astron. J.* **138**, 376 (2009).
15. If our interpretation is correct, it would not be too surprising that the first SN Ia found would be unusually luminous, because such an object would be easier to find and to recognize as such.
16. D. Kasen, *Astrophys. J.* **649**, 939 (2006).
17. P. Nugent *et al.*, *Astrophys. J.* **645**, 841 (2006).
18. X. Wang *et al.*, *Astrophys. J. Lett.* **699**, L139 (2009).
19. Poisson statistics allow fractions in the range from 0.7 to 11% (1σ).

20. T. Matheson, P. Berlind, *IAU Circ.* **7844**, 5 (2002).
21. M. W. Richmond, *et al.*, *Astron. J.* **111**, 327 (1996).
22. K. Krisciunas, *et al.*, <http://arxiv.org/abs/0908.1918> (2009).
23. A. Fiasia *et al.*, *Mon. Not. R. Astron. Soc.* **318**, 1093 (2000).
24. X. Wang *et al.*, *Astrophys. J.* **697**, 380 (2009).
25. M. Modjaz *et al.*, *Astrophys. J.* **702**, 226 (2009).
26. We thank L. Bildsten for valuable insights into the SN Ia model; A. Gal-Yam, D. Kasen, D. Maoz, T. Matheson, P. Mazzali, E. Ofek, E. Quataert, K. Shen, and N. Smith for useful discussions; R. Foley for reducing the Lick 3-m spectrum of SN 2002bj; and A. A. Miller and A. Merritt for the DeepSky analysis. A.V.F.'s group has been supported by NSF grants AST-0607485 and AST-0908886, by U.S. Department of Energy grants DE-FC02-06ER1453 (SciDAC) and DE-FG02-08ER14563, and by the TABASGO Foundation. The Katzman Automated Imaging Telescope and its ongoing operation were made possible by donations from Sun Microsystems, the Hewlett-Packard Company, AutoScope Corporation, the Lick Observatory, NSF, the University of California, the Sylvia & Jim Katzman Foundation, and the TABASGO Foundation. Some of the data presented here were obtained at the W. M. Keck Observatory, which is operated as a scientific partnership among the California Institute of Technology, the University of California, and NASA; the observatory was made possible by the generous financial support of the W. M. Keck Foundation. We thank the staffs at the Lick and Keck observatories for their assistance.

Supporting Online Material

www.sciencemag.org/cgi/content/full/1181709/DC1
SOM Text
Figs. S1 to S4
Tables S1 to S3
References

9 September 2009; accepted 29 October 2009
Published online 5 November 2009;
10.1126/science.1181709
Include this information when citing this paper.

Polarization-Induced Hole Doping in Wide-Band-Gap Uniaxial Semiconductor Heterostructures

John Simon, Vladimir Protasenko, Chuanxin Lian, Huili Xing, Debdeep Jena*

Impurity-based p-type doping in wide-band-gap semiconductors is inefficient at room temperature for applications such as lasers because the positive-charge carriers (holes) have a large thermal activation energy. We demonstrate high-efficiency p-type doping by ionizing acceptor dopants using the built-in electronic polarization in bulk uniaxial semiconductor crystals. Because the mobile hole gases are field-ionized, they are robust to thermal freezeout effects and lead to major improvements in p-type electrical conductivity. The new doping technique results in improved optical emission efficiency in prototype ultraviolet light-emitting diode structures. Polarization-induced doping provides an attractive solution to both p- and n-type doping problems in wide-band-gap semiconductors and offers an unconventional path for the development of solid-state deep-ultraviolet optoelectronic devices and wide-band-gap bipolar electronic devices of the future.

The direct-gap III-V nitride semiconductor family and its alloys span the widest spectral range of band gaps (E_g) among all semiconductors, ranging from the infrared (InN, $E_g = 0.7 \text{ eV}$) through the visible and the ultraviolet (UV) (GaN, $E_g = 3.4 \text{ eV}$) to the deep UV range (AlN, $E_g = 6.2 \text{ eV}$). This property is the basis for its applications in short-wavelength

lasers (1, 2) and in light-emitting diodes (LEDs) for solid-state lighting applications (3, 4). In addition, the wide band gaps, availability of heterojunctions, high electron-saturation velocities, and high breakdown fields enable high-speed and high-power electronic devices. Compact short-wavelength, solid-state light sources will enable a wide range of applications such as high-density

optical data storage, water treatment, sterilization of medical equipment, UV-enabled security marks on credit cards and currency bills, and biological and cellular imaging.

Currently, the III-V nitride semiconductors offer the most viable approach toward the realization of high-efficiency, deep-UV optical emitters based on semiconductors (2). A problem that has persisted since the early 1990s and is becoming increasingly troublesome is the high resistivity of p-type GaN and AlGaIn layers. The activation energy E_A of the most commonly used acceptor dopant (Mg) in GaN is $\sim 200 \text{ meV}$ (5–7), several times the thermal energy $k_B T$ at room temperature (where k_B is the Boltzmann constant, and T is temperature). The activation energy of acceptors increases with the band gap, reaching $E_A \sim 630 \text{ meV}$ in AlN (1). For comparison, the donor (Si) activation energies are $E_D \sim 15 \text{ meV}$ for GaN and $E_D \sim 282 \text{ meV}$ for AlN (1). Thus, the thermal activation of holes is highly inefficient at room temperature for GaN and becomes increasingly problematic for higher-band-gap AlGaIn and AlN layers. As a result, injection of holes is a severe impediment for light-emitting devices in

Department of Electrical Engineering, University of Notre Dame, 275 Fitzpatrick Hall, Notre Dame, IN 46556, USA.

*To whom correspondence should be addressed. E-mail: djena@nd.edu

the UV and deep-UV spectral windows. High p-type resistance leads to excessive Joule heating of p-doped AlGa_N layers for Al composition $x_{\text{Al}} \geq 20\%$. Instead, p-GaN layers must be used and absorption losses incurred in the narrower-band-gap region. Furthermore, hole reflection and trapping at heterojunction valence-band offsets block hole injection into optically active AlGa_N regions (2) and reduce the efficiency of such devices. An alternative strategy for efficient p-type doping and hole injection in wide-band-gap semiconductors is therefore highly desirable at this time.

The large ionic component of the Ga(Al)-N bonds, combined with the deviation of their equilibrium lattice structure from ideal wurtzite crystals, give rise to giant spontaneous polarization fields in III-V nitride semiconductors (8, 9). In addition, the strain-induced piezoelectric component of the fixed charge in the nitrides is the highest among all III-V semiconductors. At abrupt Al(Ga)/N/GaN heterojunctions, the sharp discontinuity in the polarization field leads to the formation of a bound sheet charge σ_{π} at the heterointerface, captured by the Gauss law boundary condition $\sigma_{\pi} = (\mathbf{P}_1 - \mathbf{P}_2) \cdot \hat{\mathbf{n}}$, where $\hat{\mathbf{n}}$ is the unit vector normal to the heterointerface, and $(\mathbf{P}_1, \mathbf{P}_2)$ are the polarization fields across the heterojunction. When wurtzite nitride crystals are grown along the [0001] orientation (metal or

Ga-face), a positive bound polarization charge creates a high electric field and energy-band bending, such that a mobile two-dimensional electron gas (2DEG) forms at AlGa_N/GaN heterojunctions without the need for intentionally introduced impurity dopants. The bound sheet-charge density can be as high as $\sigma_{\pi} \sim 6 \times 10^{13} \text{ cm}^{-2}$ at pseudomorphic AlN/GaN heterojunctions, facilitating mobile 2DEGs with a very high charge carrier density. For example, in AlN/GaN semiconductor heterostructures, the mobile 2DEG concentrations are $4 \times 10^{13} \text{ cm}^{-2}$ (10). Such polarization-induced 2DEGs form the basis of nitride high-electron mobility transistors that have surpassed transistors made from any other semiconductor family in RF power performance (11).

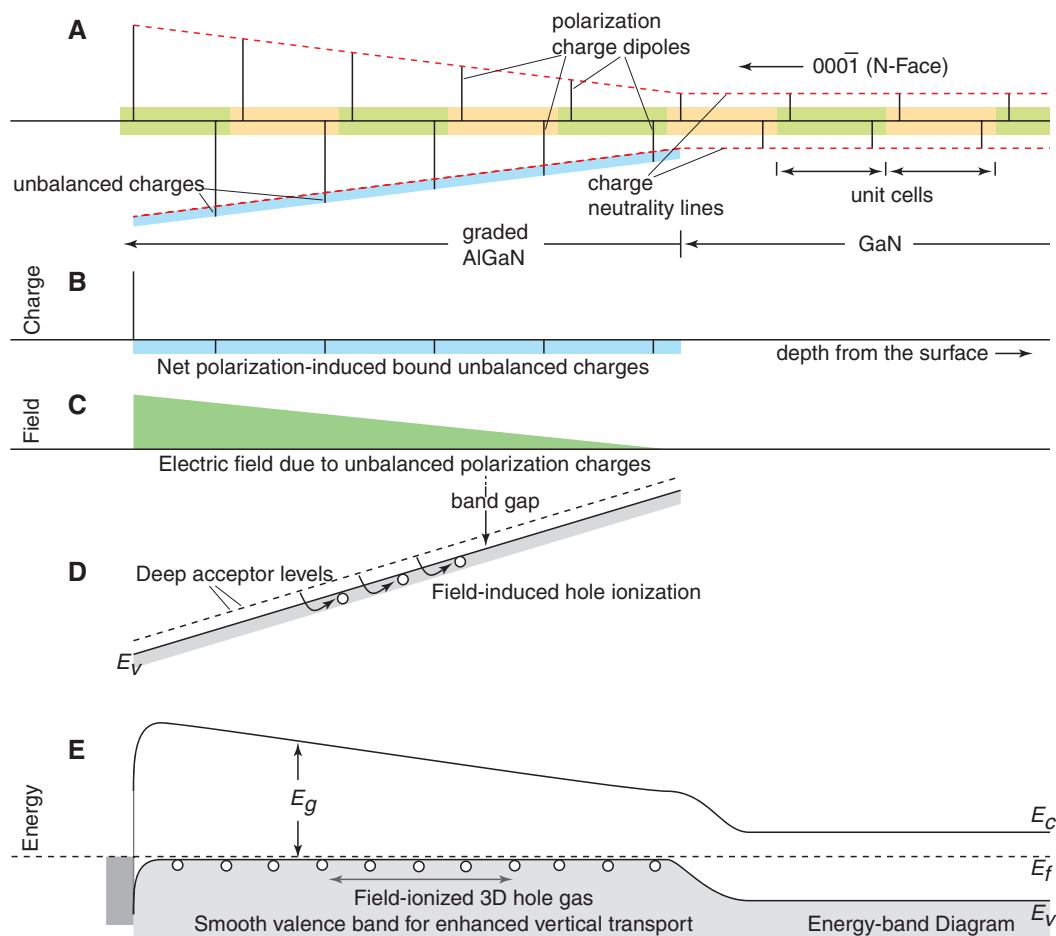
The polarization fields have also been exploited to create parallel sheets of 2D hole gases in Mg-doped AlGa_N/GaN multiple-quantum-well structures (12, 13). Although such parallel 2D hole sheets have high conductivity in the plane of the heterojunctions, they suffer from low conductivity perpendicular to the interfaces because of potential barriers in the valence band that require transport to occur through tunneling or thermionic emission processes. Even in short-period superlattice structures, the large effective mass of holes in minibands results in low mobility and high resistance (1). An alternate strat-

egy for hole doping without potential barriers will facilitate higher conductivities.

If instead of sharp heterojunctions we grow a compositionally graded crystal, the bound polarization-induced sheet charge spreads to a bound 3D form in accordance with $\rho_{\pi}(z) = -\nabla \cdot \mathbf{P}(z)$, where $\rho_{\pi}(z)$ is the volume charge density in the polar (z) direction, and $\nabla \cdot$ is the divergence operator. For [0001]-oriented Ga-face crystals graded from GaN to AlGa_N, the polarization bound charge is positive and induces the formation of a mobile 3D electron gas. These 3D electron slabs are quite distinct from those formed by donor impurity doping: Because the carriers are created by effective electrostatic “field” ionization, they require no impurity incorporation, and thus exhibit virtually no freezeout at cryogenic temperatures as opposed to thermally ionized carriers in shallow, donor-doped layers (14). The resulting 3D electron gases have higher n-type conductivity than impurity-doped layers of comparable carrier concentration, because ionized impurity scattering is absent. The absence of freezeout and high mobilities made it possible to observe Shubnikov–de Haas oscillations (15). Polarization-induced field-effect transistors have also been demonstrated recently with this technique (16).

By the same measure, flipping the polarity of the crystal (growing along the N-face, which is

Fig. 1. Schematic illustration of polarization-induced p-type doping in graded polar heterostructures. (A) Sheets of charge dipoles in every unit cell of the crystal. The net unbalanced polarization charge is shown in (B), which leads to the electric field in (C), and the energy-band bending in the valence band in (D) if holes are not ionized. Field ionization of holes results in a steady-state energy-band diagram shown in (E), which highlights the smooth valence-band edge without any potential barriers for hole flow. E_f is the Fermi level; E_c and E_v are the conduction and valence-band edges, respectively; and E_g is the band gap.



the $[000\bar{1}]$ direction) and compositional grading from GaN to AlGaN should result in mobile 3D hole slabs. The ability to do so without the introduction of Mg-acceptor dopants hinges on the propensity of the surface to act as a remote acceptor state. The surface of III-V nitride semiconductors freely provides mobile electrons, but not holes, and this difference has been attributed to the presence of deep-level traps that localize holes (17). Lowering of defect and trap densities may enable dopant-free p-type carriers, but intentionally introducing Mg-acceptor dopant atoms in the N-face graded AlGaN layer serves as the necessary source of holes. This work demonstrates the ability to use the polarization charges

in N-face $[000\bar{1}]$ layers to generate polarization-induced, p-type graded AlGaN slabs that are highly conductive.

The mechanism of polarization-induced hole formation is illustrated schematically in Fig. 1. The total polarization (spontaneous plus piezoelectric) can be pictured as charge dipoles in every unit cell of the crystal (Fig. 1A). Because $\text{Al}_x\text{Ga}_{1-x}\text{N}$ (where x is the Al mole fraction) has higher polarization than GaN, the sheet-charge dipoles in unit cells of the AlGaN layer are of a higher magnitude than in GaN, so the dipole strength increases linearly with the composition. When the composition of the layer is graded with increasing Al mole fraction, the net unbalanced

bound polarization charge is negative (Fig. 1B), given by $\rho_\pi(z) = -\nabla \cdot \mathbf{P}(z) \sim 5 \times 10^{13} \times (x_2 - x_1)/d \text{ cm}^{-3}$, where x_1 and x_2 are the Al compositions at the ends of the graded layer of thickness d (in centimeters). This bound charge creates a built-in electric field (Fig. 1C) and energy-band bending that would be greater than the band gap of the semiconductor layer if left uncompensated (Fig. 1D). To neutralize the bound, negative polarization charge, holes are consequently field-ionized from the deep Mg-acceptor atoms and form a high-density mobile 3D hole gas. The concentration of the 3D hole gas should then exhibit a weak temperature dependence and resist freezeout at low temperatures. In addition, the

Fig. 2. Structural and transport properties of p-type samples (A) Concentration of Al and Ga atoms in a compositionally graded AlGaN sample (sample d), with the measured concentration of Mg dopant atoms. The thickness of the graded layer is $d \sim 85 \text{ nm}$, capped with a thin, heavily doped p++ layer for ohmic contacts. SIMS, secondary ion mass spectrometry. (B) Measured temperature-dependent resistivity for samples a to c, highlighting the polarization boost in p-type conductivity.

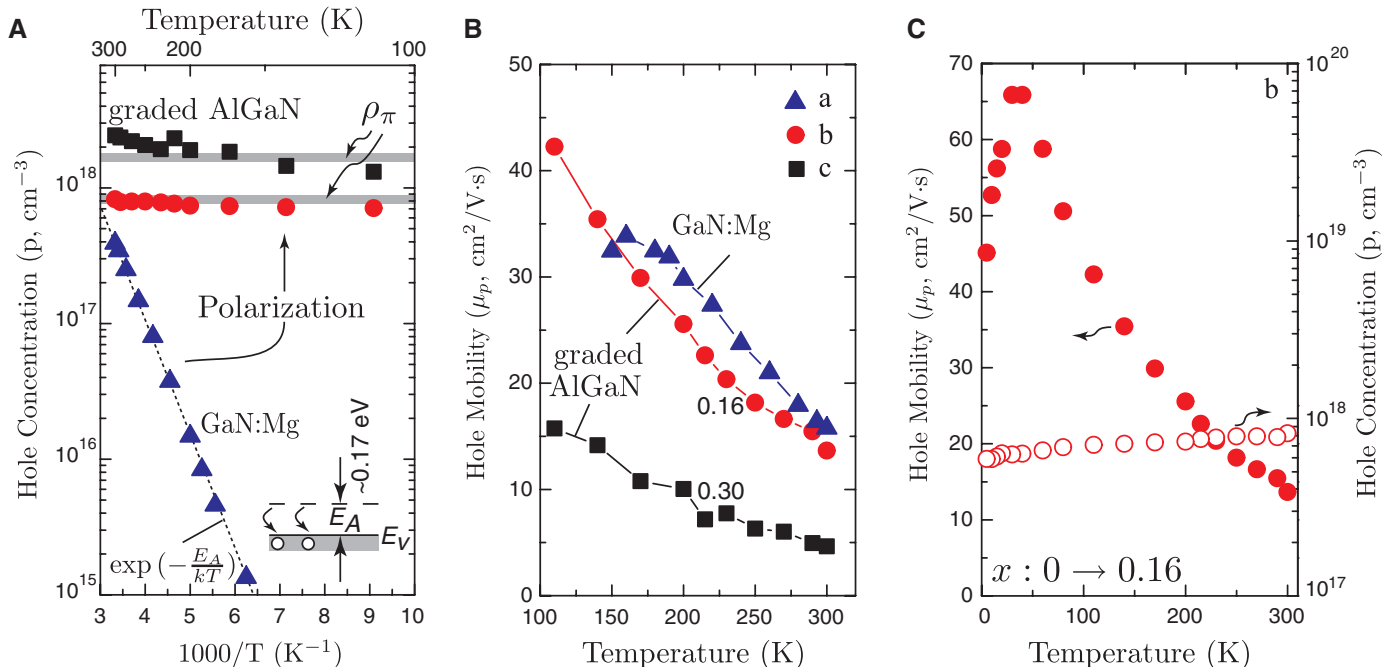
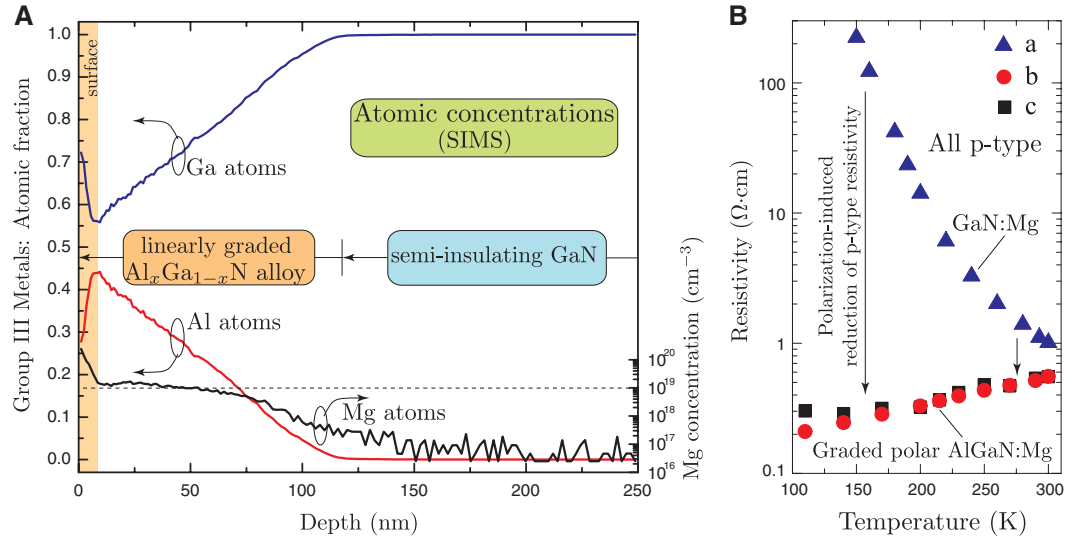


Fig. 3. Hall-effect temperature-dependent (A) hole concentration, (B) hole mobilities, and (C) hole concentration and mobility measured down to $T = 4 \text{ K}$. The polarization-doped graded AlGaN p-type layers show higher hole

concentrations and conductivities. Holes in polarization-doped layers are resistant to freezeout at low temperatures, and their mobility and concentration can be measured down to cryogenic temperatures.

smooth spatial variation of the valence-band edge (Fig. 1E) should further facilitate high-conductivity p-type transport in both lateral and vertical directions.

To test this concept of polarization-induced p-type doping, Mg-doped graded AlGaIn layers were grown on top of semi-insulating N-face [000 $\bar{1}$] GaN substrates by plasma-assisted molecular beam epitaxy. A Mg-doped GaN sample ($N_a \sim 10^{19}/\text{cm}^3$, sample a; here, N_a is the acceptor concentration) was used as a control sample. Graded AlGaIn samples doped with the same Mg concentration but linearly graded from $x = 0$ to 0.16 (sample b) and $x = 0$ to 0.3 (sample c) over $d \sim 85$ nm were grown. The sample structures and compositions were characterized by x-ray diffraction, in situ reflection, high-energy electron diffraction patterns and atomic force microscopy [see supporting online material (SOM) for a description of crystal growth and characterization (18)]. Secondary ion mass spectrometry measurements were performed on a separate graded AlGaIn sample ($x = 0$ to 0.4, sample d) as well as the control Mg-doped GaN sample to verify the incorporation of Mg atoms into the crystal and the linear grading of Al composition in the polarization-doped AlGaIn layers (Fig. 2A). Samples a to c were subsequently processed for Hall-effect measurements, as described in the SOM (18).

The measured resistivities of the bulk p-GaN and polarization-doped AlGaIn layers from $T = 300$ to 100 K are shown in Fig. 2B. The room-temperature resistivity of both polarization-doped samples b and c ($\rho_b, \rho_c \sim 0.6$ ohm-cm) is lowered by more than a factor of 2 compared with that of the control sample a ($\rho_a \sim 1.22$ ohm-cm). The

resistivity of the control sample a increased monotonically by more than two orders of magnitude as the temperature was lowered from 300 to 100 K (Fig. 2B); this increase is expected from the freezeout of thermally activated holes. In comparison, the resistivities of the polarization-doped samples b and c actually decreased with temperature, which is indicative of metallic behavior. This decrease in resistivity can occur if (i) polarization-induced holes do not freeze out at low temperatures and (ii) the mobilities of polarization-induced holes increase when temperature is lowered from 300 to 100 K.

Temperature-dependent Hall-effect measurements performed at a magnetic field of 0.5 T confirmed the two hypotheses. The measured hole concentrations and mobilities are shown in Fig. 3, A and B. Compared with the exponential freeze-out (activation energy $E_A \sim 170$ meV) of mobile holes for the Mg-doped GaN control sample (a), the hole densities in the polarization-induced graded AlGaIn samples (b and c) remain essentially independent of temperature, and are near the theoretical prediction [$p_\pi \sim 5 \times 10^{13} \times (x_2 - x_1)/d \text{ cm}^{-3}$], as indicated by the thick gray lines in Fig. 3A. Polarization charges are atomic in origin and do not require thermal energy to be activated, so they enhance the hole concentration independent of temperature. In addition, because polarization charges are spatially distributed, the band-edge potential variations are smooth, and no abrupt potential barriers exist for the flow of holes along any direction. These properties are a major advantage and novelty of this method of p-type doping. Polarization enhancement of hole densities are 2 \times and 6 \times for samples b and c at room temperature and many orders of magnitude at lower temperatures.

The measured hole mobilities as a function of temperature in samples a to c are shown in Fig. 3B. Sample c has lower hole mobility because of increased alloy scattering. Although it was not possible to perform Hall-effect measurements for control sample a below $T \sim 150$ K because of carrier freezeout, we measured the polarization-enhanced hole concentration and mobility down to $T = 4$ K for sample b. As shown in Fig. 3C, the hole concentration showed a very small decrease with temperature, whereas the hole mobility increased to $\mu_p \sim 65 \text{ cm}^2/\text{V}\cdot\text{s}$ at 30 K before decreasing, indicating competition between phonon and impurity scattering.

To test the effectiveness of such polarization-enhanced p-type layers as hole injectors in optical devices, a Mg-doped graded AlGaIn layer ($x = 0$ to 30%, identical to sample c) was grown on a n-type doped N-face [000 $\bar{1}$]-oriented GaN substrate. A control p-n junction with a Mg-doped GaN p-type layer was also grown, and these structures were fabricated into light-emitting diode structures [see SOM for the fabrication procedure (18)]. These junctions serve as prototype LEDs, requiring electrical injection of holes and electrons into the depletion region where they recombine radiatively to emit photons. Under forward bias at room temperature, both devices exhibit electroluminescence in the UV spectral range (Fig. 4A). We observed characteristic sub-band-gap emission attributed to deep acceptor levels in nitrides (19). Furthermore, we note that the graded AlGaIn p-layer structure showed much brighter optical emission (Fig. 4B), which we attribute to two factors: (i) improved p-type conductivity in the vertical direction due to polarization-induced hole doping and (ii) the existence of a built-in quasi-

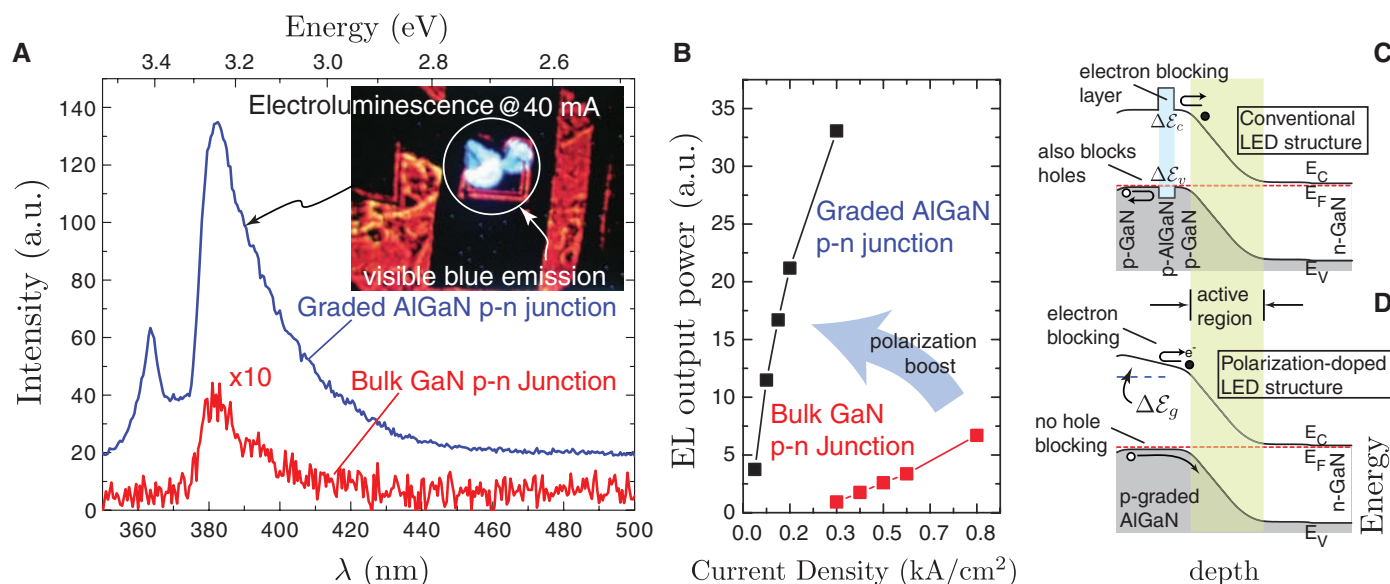


Fig. 4. (A) Room temperature electroluminescence of the graded p-type AlGaIn junction and the control GaN p-n junction at 40-mA drive current. Both samples have an area of 80 μm by 150 μm . (Inset) Optical microscope micrograph displaying the blue part of the emission of the graded AlGaIn junction. a.u., arbitrary units. (B) Relative output intensity with increasing drive current for the graded AlGaIn p-n junction and the control bulk-doped p-n junction. The

polarization-doped diode shows much brighter emission than the bulk-doped p-n junction. Schematic energy-band diagrams of a conventional (C) LED device and (D) a polarization-doped device. The graded AlGaIn p-n junction uses the entire band offset ΔE_g in the conduction band as an electron-blocking layer, resulting in enhanced electroluminescence. In comparison, a traditional electron-blocking layer (C) also blocks holes through a valence-band offset ΔE_v .

electric field imposed on minority electrons injected into the p-type layer of the graded AlGaIn. The compositional grading in the p-type AlGaIn layer causes the increase in the band gap ΔE_g to appear entirely in the conduction band, which acts as a natural electron-blocking layer. This feature is shown in the energy-band diagram in Fig. 4D. Electron-blocking layers have been shown to improve the efficiency of emission by preventing the spillover of higher mobility electrons from the optically active regions of nitride LEDs (20). Conventional electron-blocking layers implemented in nitride LEDs and lasers consist of a thin AlGaIn layer placed on the p-doped side [schematic band diagram shown in Fig. 4C]. In addition to blocking electron overflow through a conduction band barrier ΔE_C , such layers also prevent efficient hole injection because of the unavoidable valence-band offset ΔE_V (21). Polarization-doped graded layers provide a solution to this design bottleneck. In addition to improving the p-type conductivity, the polarization-induced graded p-type AlGaIn layer facilitates electron blocking without adding barriers to hole injection and offers an added degree of freedom in graded-refractive-index design, all of which are useful for UV laser applications. The polarization-doped layer is also of a larger band gap than the active region of the p-n junction and serves as a natural optically transparent layer with minimal absorption losses.

This method of polarization doping should prove particularly useful for deep-UV optoelectronic applications where both p- and n-type doping of high Al composition AlGaIn is a major challenge. The technique presented here could be applied to produce highly conductive p-type regions in wide-band-gap nitrides composed of high-Al composition AlGaIn and in the more general AlInGaIn material system with proper choice of the crystal direction of growth and management of strain within allowable limits. The doping scheme can be used to obtain desired hole or electron concentrations in spite of poor ionization efficiencies of deep-level dopants in any semiconductor crystals that possess sufficiently strong spontaneous and piezoelectric polarization (for example, in the ZnO material family).

References and Notes

1. Y. Taniyasu, M. Kasu, T. Makimoto, *Nature* **441**, 325 (2006).
2. A. Khan, K. Balakrishnan, T. Katona, *Nat. Photonics* **2**, 77 (2008).
3. D. A. Steigerwald *et al.*, *IEEE J. Sel. Top. Quantum Electron.* **8**, 310 (2002).
4. O. Brandt, K. H. Ploog, *Nat. Mater.* **5**, 769 (2006).
5. P. Kozodoy *et al.*, *J. Appl. Phys.* **87**, 1832 (2000).
6. W. Götz, N. M. Johnson, J. Walker, D. P. Bour, R. A. Street, *Appl. Phys. Lett.* **68**, 667 (1996).
7. C. J. Eiting, P. A. Grudowski, R. D. Dupuis, *Electron. Lett.* **33**, 1987 (1997).

8. F. Bernardini, V. Fiorentini, D. Vanderbilt, *Phys. Rev. B* **56**, R10024 (1997).
9. C. Wood, D. Jena, *Polarization Effects in Semiconductors: From Ab-Initio Theory to Device Applications* (Springer, New York, 2007).
10. Y. Cao, D. Jena, *Appl. Phys. Lett.* **90**, 182112 (2007).
11. Y.-F. Wu *et al.*, *IEEE Electron Device Lett.* **25**, 117 (2004).
12. I. D. Goepfert, E. F. Schubert, A. Osinsky, P. E. Norris, *Electron. Lett.* **35**, 1109 (1999).
13. P. Kozodoy, M. Hansen, S. P. DenBaars, U. K. Mishra, *Appl. Phys. Lett.* **74**, 3681 (1999).
14. J. Simon, A. K. Wang, H. Xing, S. Rajan, D. Jena, *Appl. Phys. Lett.* **88**, 042109 (2006).
15. D. Jena *et al.*, *Phys. Rev. B* **67**, 153306 (2003).
16. S. Rajan, H. Xing, S. DenBaars, U. K. Mishra, D. Jena, *Appl. Phys. Lett.* **84**, 1591 (2004).
17. S. Rajan *et al.*, *Appl. Phys. Lett.* **102**, 044501 (2007).
18. Details of the growth and fabrication procedure are described in the supporting online material.
19. F. Calle *et al.*, *MRS Internet J. Nitride Semicond. Res.* **3**, article 24 (1998).
20. R.-C. Tu *et al.*, *IEEE Photon. Technol. Lett.* **15**, 1342 (2003).
21. S.-H. Han *et al.*, *Appl. Phys. Lett.* **94**, 231123 (2009).
22. We thank the U.S. Office of Naval Research and the NSF (award no. 0907583) for financial support and C. Wood for discussions. N-face semi-insulating substrates were obtained from D. Hanser, Kyma Technologies, Raleigh, North Carolina.

Supporting Online Material

www.sciencemag.org/cgi/content/full/327/5961/60/DC1
Materials and Methods
Figs. S1 to S3
References

12 October 2009; accepted 30 October 2009
10.1126/science.1183226

Translocation of Single-Stranded DNA Through Single-Walled Carbon Nanotubes

Haitao Liu,^{1*} Jin He,^{2*} Jinyao Tang,¹ Hao Liu,^{2,3} Pei Pang,^{2,4} Di Cao,^{2,4} Predrag Krstic,⁵ Sony Joseph,⁵ Stuart Lindsay,^{2,3,4†} Colin Nuckolls^{1†}

We report the fabrication of devices in which one single-walled carbon nanotube spans a barrier between two fluid reservoirs, enabling direct electrical measurement of ion transport through the tube. A fraction of the tubes pass anomalously high ionic currents. Electrophoretic transport of small single-stranded DNA oligomers through these tubes is marked by large transient increases in ion current and was confirmed by polymerase chain reaction analysis. Each current pulse contains about 10^7 charges, an enormous amplification of the translocated charge. Carbon nanotubes simplify the construction of nanopores, permit new types of electrical measurements, and may open avenues for control of DNA translocation.

We report the use of single-walled carbon nanotubes (SWCNTs) as nanopores for analyzing molecular transport properties. Nanopores are orifices of molecular diameter that connect two fluid reservoirs. At this length scale, the passage of even a single molecule generates a detectable change in the flow of ionic current through the pore (1, 2). They can be used as single-molecule Coulter counters and form the basis of proposed new approaches to DNA sequencing (3). The first nanopore devices were based on pore proteins (4–7), but more

recently pores have been fabricated by drilling (and sometimes partially refilling) solid-state materials (8–12). Nanochannels have been formed by etching silicon nanowires (13), and channels with one nanoscale dimension have been etched into glass (14) or quartz (15).

Carbon nanotubes are obvious candidates for the fabrication of nanopore structures. Pressure-driven gas, water, and ion transport has been recorded through membranes composed of many multiwalled carbon nanotubes (16) or double-walled carbon nanotubes (17). These experi-

ments showed that the water flow rate is greatly enhanced inside the tube, an effect confirmed by molecular dynamics simulations (18). DNA has been passed through a 100-nm diameter carbon nanotube (19) and 50-nm-wide hydrophilic channels (13). It seems counterintuitive that hydrophilic DNA would enter the hydrophobic interior of a SWCNT, but simulations show that both RNA (20) and DNA (21) will translocate through 1.5- to 2-nm diameter tubes. The simulations were carried out using very large electric fields (tenths of a volt per nm) to generate observable motion on the simulation time scale. This result leaves open the possibility that some measurable translocation might occur at the much smaller fields that could be implemented in the laboratory. Here, we report direct measurement of this translocation.

We have made a device in which one SWCNT spans a barrier between two fluid reservoirs [see Fig. 1 and Supporting Online Material (22)]. Relative to CNT membranes (16, 17), this arrangement makes it possible to detect signals from the translocation of a single molecule and to correlate

¹Department of Chemistry, Columbia University, New York, NY 10027, USA. ²Biodesign Institute, Tempe, AZ 85287, USA. ³Department of Chemistry and Biochemistry, Tempe, AZ 85287, USA. ⁴Department of Physics, Arizona State University, Tempe, AZ 85287, USA. ⁵Physics Division, Oak Ridge National Laboratory, Oak Ridge, TN 37831, USA.

*These authors contributed equally to this work.

†To whom correspondence should be addressed. E-mail: Stuart.Lindsay@asu.edu (S.L.); cn37@columbia.edu (C.N.)